A Multi-Channel Software Decoder for the LoRa Modulation Scheme

Pieter Robyns[1], Peter Quax[2], Wim Lamotte[1], William Thenaers[3]
[1]*Hasselt University - tUL, Expertise centre for Digital Media, Martelarenlaan 42, 3500 Hasselt, Belgium*
[2]*Hasselt University - tUL - Flanders Make, Expertise centre for Digital Media, Martelarenlaan 42, 3500 Hasselt, Belgium*
[3]*Hasselt University - tUL, Martelarenlaan 42, 3500 Hasselt, Belgium*
[1,2]*{firstname.lastname}@uhasselt.be,* [3]*william.thenaers@student.uhasselt.be*

Keywords: LoRa, Software Defined Radio, PHY layer, decoder, signal processing, reverse engineering

Abstract: LoRa is a recently introduced modulation scheme specifically designed for Low-Power Wide-Area Networks. In this paper, we provide the first detailed and complete description of the LoRa PHY layer, and present a novel methodology for detecting and decoding LoRa frames using Software Defined Radios. Our proposed decoding approach can efficiently decode multiple channels simultaneously in software due to an invariance towards the signal frequency. Hence, our approach also removes the need for correcting frequency offset errors imparted by the transmitter or receiver. We have evaluated our decoding technique in a lab setup using three Software Defined Radios (USRP B210, HackRF, and RTL-SDR) and three commercial off-the-shelf hardware LoRa transceivers (Microchip RN2483, HopeRF RFM96, and Semtech SX1272). We show that our decoder is fully compatible with all configurations of the RN2483 and SX1272, achieving an overall packet error rate of 0 for a signal-to-noise ratio of 20 dB. The source code of the decoder and datasets used in the evaluation are made available publicly.

1 INTRODUCTION

In coming years, the industry is expected to show an increased interest in Low-Power Wide-Area Networks (LPWANs) and their applications, such as smart metering, location tracking, Wireless Sensor Networks (WSNs), smart transportation systems and health monitoring (i-SCOOP, 2017). In such networks, several low-power embedded devices are typically deployed in areas of interest, and perform Machine to Machine (M2M) communication or interact with services on the internet in order to complete a certain computing task. For example, an internet-connected embedded device may be distributed to individuals suffering from a cardiovascular disease, so that their condition can be monitored in real time by doctors.

The heightened attention for these use cases sparked the creation of several Physical (PHY)-layer modulation protocols that are optimized for LPWANs, i.e. for low power consumption and long range communications. Examples of these protocols are LoRa (LoRa Alliance, 2017), Sigfox (Sigfox, 2017), Wi-Fi HaLow (Wi-Fi Alliance, 2017), LTE-M (3GPP, 2017), and Weightless (Weightless, 2017). Out of those, LoRa is a proprietary, low-power, and long-range modulation scheme developed by Cycleo and acquired by Semtech in 2012 (Semtech, 2012). It is currently among the more popular protocols, with numerous gateways already deployed on a global scale (The Things Network, 2017).

Due to its proprietary nature, specialized hardware is required in order to transmit or receive LoRa messages. Examples of such hardware are the SX1272 transceiver developed by Semtech (Semtech, 2015b) and the RN2483 transceiver developed by Microchip (Microchip Technology Inc., 2015). Both transceivers expose a serial interface to the user. The serial interface can only be used to make high level configuration changes to the LoRa modem, and to transmit or receive payloads using LoRa modulation. Hence, the entire PHY layer of these transceivers is abstracted in hardware, and therefore cannot be accessed or modified.

Having access to the PHY layer of a wireless protocol is a desirable feature with many interesting use cases for research and development. For example, recent works have demonstrated the possibility to fingerprint individual transceivers using only PHY-layer properties of the signal (Danev et al., 2012; Robyns et al., 2017; Vo-Huu et al., 2016). This could be useful for tracking devices or intrusion detection. Another use case could be to perform software simulations of the PHY layer, e.g. to determine the effect of various channel conditions without requiring multiple physical deployments of hardware transceivers (Ben Hamida et al., 2009; Mezzavilla et al., 2015). As a final example, enabling modifications to the PHY layer allows for rapid prototyping of improvements in terms of security, performance or reliability (Bloessl et al., 2013a; Sklivanitis et al., 2016).

In this paper, we provide several contributions that aim to bring the advantages of PHY-layer access to the LoRa modulation scheme. First, we provide a detailed description of the LoRa PHY layer. This description includes newly added and undocumented features of the LoRa specification that were reverse engineered from hardware LoRa transceivers. To the best of our knowledge, we are the first to provide a complete and validated overview. Second, we present our algorithms for the detection, synchronization, and decoding of raw PHY-layer LoRa frames using Software Defined Radios (SDRs). These algorithms include a novel decoding approach and a novel clock drift correction approach for LoRa, both implemented in a complete and open-source software LoRa decoder using the GNU Radio framework. Our decoder is capable of decoding multiple channels simultaneously in real time regardless of the frame's network identifier, similar to the capabilities of "monitoring mode" devices in context of 802.11 (Wi-Fi). Finally, we evaluate our decoder in a lab setup, and show that it can interoperate with hardware LoRa transceivers, using only inexpensive Commercial Off-The-Shelf (COTS) SDRs such as the RTL-SDR.

The structure of this paper is as follows. In Section 2, we will present an overview of the LoRa PHY layer in consideration of our first contribution. Section 3 then shows how this knowledge can be applied to build a complete software LoRa decoder. In addition, we detail our novel demodulation and clock drift correction approaches. Our decoder will be compared in terms of compatibility with existing LoRa hardware and accuracy in Section 4, followed by a discussion of these results. Works related to this research will be discussed in Section 5. Finally, in Section 6, we will make concluding remarks and give directions for future work in this area of research.

2 LoRa PHY Layer

In order to correctly decode LoRa-modulated data, a receiver must sequentially perform seven operations on the PHY layer, namely detection, synchronization, demodulation, deinterleaving, dewhitening, decoding, and packet construction. A partial description of these operations can be found in several technical reports released by Semtech (Seller and Sornin, 2014; Semtech, 2015b; Sornin et al., 2015; Semtech, 2015a) and in the paper presented by Goursaud et al. (Goursaud and Gorce, 2015). However, the information contained within these works is insufficient to build a decoder that can interoperate with real hardware LoRa transceivers. To this end, we have reverse engineered a RN2483 LoRa transceiver, and provide the first complete overview of the LoRa PHY layer in this section.

2.1 Modulation

The LoRa modulation scheme is based on Chirp Spread Spectrum (CSS) modulation (Goursaud and Gorce, 2015), and defines a "chirp" as a single symbol (Semtech, 2015a). A standard, unmodulated linear chirp is called a "base chirp", and can be mathematically described in function of the time t as follows (Mann and Haykin, 1991):

$$x(t) = e^{i(\varphi_0 + 2\pi(\frac{k}{2}t^2 + f_0 t))} \tag{1}$$

where φ_0 is the initial phase, k is the rate of frequency change, and f_0 is the initial frequency. Given the channel bandwidth BW, the parameters f_0 and k are set so that the frequency increases from $f_0 - \frac{BW}{2}$ to $f_0 + \frac{BW}{2}$ over the duration T of the chirp. Hence, $f_0 = -\frac{BW}{2}$ and $k = \frac{BW}{T}$. Here, the chirp duration T depends on the bandwidth of the signal and on a parameter called the Spreading Factor (SF) according to the relation $T = \frac{2^{SF}}{BW}$ (Seller and Sornin, 2014).

Given that $x(t + nT) = x(t)$ with $n \in \mathbb{N}$, an integer value $i \in \{0,1\}^{SF}$ can be modulated onto the base chirp by introducing a time shift of $\hat{t} = \text{Gray}^{-1}(i)\frac{T}{2^{SF}}$ to the signal in Equation 1, where Gray^{-1} stands for a Gray decoding operation (Gray, 1953). This way, a symbol is essentially quantized into 2^{SF} time shift bins divided over the bandwidth, called "chips", that determine i. Upon reception of a modulated chirp with an unknown time shift $x(t + \hat{t})$, the chip value i can be recovered by sampling the signal at the chip rate and calculating:

$$i = \text{Gray}(\arg\max(\left|\text{FFT}(\ x(t+\hat{t}) \odot \overline{x(t)}\ )\right|\ )\ ) \tag{2}$$

where $\overline{x(t)}$ denotes the conjugate of a base chirp, the $\odot$ operator indicates element-wise multiplication, $\left|\text{FFT}(x)\right|$ signifies the magnitude of the Fast Fourier Transform (FFT) of x, and Gray stands for Gray encoding. Figure 1 shows an example where a value of

$i = 20$ is modulated onto the base chirp, shifting it by 192 samples.

2.2 Interleaving

When using the modulation approach described above, errors can be introduced due to noise, interference, and time or frequency offsets. These errors cause the receiver to derive an incorrect chip value from the modulated symbol. For example, a burst of noise could cause the peak of the FFT spectrum to appear at a different chip, therefore corrupting the entire chip value.

In order to limit the impact of bursty noise to a single bit error per symbol, multiple chip values are stacked together such that a bit matrix $\{0,1\}^{SF\times(4+CR)}$ is obtained. Here, the Coding Rate (CR) or equivalently, the number of parity bits, can range from 1 to 4. For example, when using $SF = 7$ and $CR = 4$, we obtain a matrix $\{0,1\}^{7\times 8}$ as shown in Figure 2. A codeword of $4+CR$ bits is then obtained by diagonally deinterleaving the matrix. As such, the first chip value provides all first Least Significant Bits (LSBs) of the codewords, the second chip value provides all second bits of the codewords, etc. The direction of the interleaving diagonal appears to be upwards in practice, in contrast to the LoRa patent where the interleaving diagonal direction is downwards[1] (Seller and Sornin, 2014). Observe that as a result of the interleaving operation, an entirely corrupted chip value now only affects one bit per codeword.

The LoRa specification also defines a "reduced rate" mode, in which the top two rows of the interleaving matrix are discarded. Consequently, the dimensions of the matrix become $\{0,1\}^{SF-2\times(4+CR)}$, yielding two codewords less after deinterleaving. The discarded rows correspond to the LSBs of the chip values, which are more prone to errors because they correspond to narrower frequency bins in the FFT spectrum. Therefore, in reduced rate mode, a decreased data rate is traded for an increased robustness to noise. The PHY layer header of LoRa frames is always transmitted in reduced rate mode, whereas the payload bytes are only transmitted in reduced rate mode when SF 11 or SF 12 is used (Semtech, 2015b, p. 28, 112).

2.3 Coding

After deinterleaving, a number of codewords of size $4+CR$ are obtained by the receiver. The codewords of the frame payload are "whitened" in order to keep the data Direct Current (DC)-free (Semtech, 2015b, p. 75). Here, whitening is defined as an operation where the data is XOR-ed with a 9-bit Linear Feedback Shift Register (LFSR) after synchronization (Semtech, 2015b, p. 72). The used coding algorithm is not explicitly mentioned in the patent or chipset datasheet (Seller and Sornin, 2014; Semtech, 2015b), leaving this an open choice to the vendor.

For the transceivers we considered during our tests (see Section 3), we have reverse engineered the coding scheme and discovered that a modified version of $4/(4+CR)$ Hamming coding is utilized in practice. Hence, each codeword results in 4 data bits when decoded, which are subsequently parsed according to the LoRa frame structure. In Section 3.3, we will discuss our approach for decoding the data further.

2.4 Frame Structure

On the PHY layer, LoRa defines a frame structure with the following sequentially transmitted fields (Semtech, 2015b, p. 27–29):

- **Preamble**: A variable-sized sequence of base chirps that is used for time and frequency synchronization.
- **Frame synchronization symbols**: Two modulated chirps whose value can be used as a network identifier. A hardware LoRa transceiver will drop frames containing synchronization symbols that do not match a preconfigured value.
- **Frequency synchronization symbols**: Two conjugate base chirps followed by a conjugate chirp with duration $\frac{T}{4}$, which can both be used for fine frequency synchronization.
- **Header (optional)**: Field containing the payload length, used data rate, a bit indicating the presence of a payload Cyclic Redundancy Check (CRC), and 1-byte header checksum. A CR of 4 is always used in combination with reduced rate mode for the header[2] (Seller and Sornin, 2014). The header can be explicitly transmitted (*explicit* mode) or left out of the frame (*implicit* mode). In the latter case, the transmitter and receiver must configure the coding rate and CRC presence bit beforehand.
- **Payload**: Variable-length field containing the transmitted Medium Access Control (MAC) layer data and a 2-byte CRC of this data.

Figure 3 shows an example LoRa signal and its frame structure.

[1]Note that this has no impact on the decoding performance.

[2]Since the header contains the payload length and coding rate, it is essential that these fields are decoded correctly. Hence the increased robustness measures.

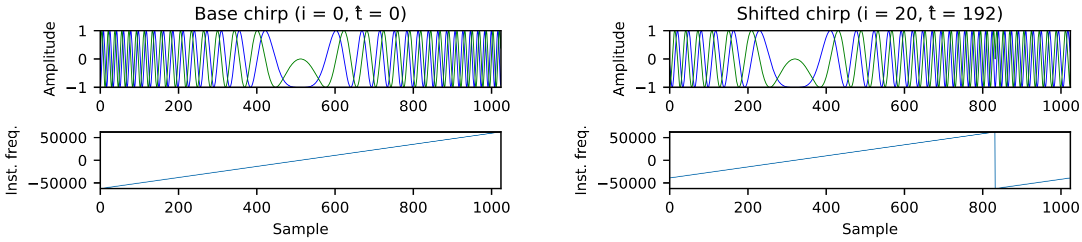

Figure 1: Example of an unmodulated LoRa base chirp and a chirp modulated with $i = 20$. The top row of figures shows the time domain complex signal, whereas the bottom row of figures shows the instantaneous frequencies of the signals in Hz.

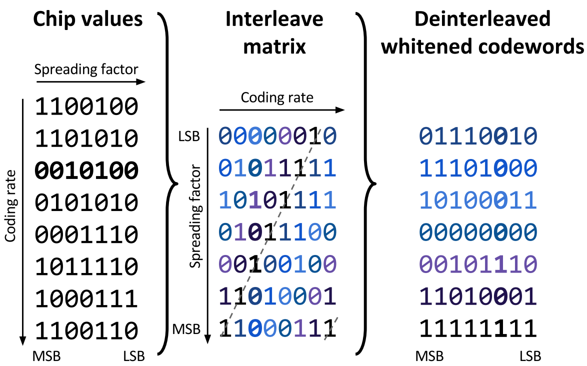

Figure 2: Diagonal deinterleaving with $SF = 7$ and $CR = 4$. The bits of the third chip value are shown in bold.

2.4.1 Header Structure

The exact length and bit order of the fields in the PHY layer header are not explicitly stated in the specifications. However, since the transmission of an explicit header requires a SF of at least 7, and the header is always transmitted with $CR = 4$ at a reduced rate (Seller and Sornin, 2014), the header must fit in an interleaving matrix of $\{0,1\}^{(7-2)\times 8}$. Therefore, the header length must be equal to 5 codewords of 8 bits, i.e. 40 bits in total. Any remaining bits in the interleaving matrix are used for the payload.

After decoding, the header data thus has a length of $40 \cdot \frac{4}{8} = 20$ bits or 2.5 bytes. We have experimentally determined that when transmitting data using a Microchip RN2483 LoRa transceiver, the left-to-right order of the PHY header is as follows: a single payload `Length` byte, followed by a nibble for the CR and MAC CRC presence, the High Nibble (HN) of the header checksum, and finally the Low Nibble (LN) of the header checksum[3]. An overview of these fields is given in Figure 4.

[3] Only the 5 LSBs of the checksum byte appear to be used in practice.

3 SOFTWARE DEMODULATOR

We have implemented the complete PHY layer of LoRa in software, using the open source GNU Radio signal processing framework. The source code of the decoder is publicly available on Github[4]. An overview of the decoder components is given in Figure 5.

3.1 Detection and Synchronization

As a first step in the demodulation process, the receiver must detect the LoRa preamble. To this end, we exploit the repeating property of the preamble by using the Schmidl-Cox algorithm, which defines two quantities $P(d)$ and $R(d)$ as follows (Schmidl and Cox, 1997):

$$P(d) = \sum_{m=0}^{L-1} (x^*_{t+m}\, x_{t+m+L}) \tag{3}$$

$$R(d) = \sum_{m=0}^{L-1} |x_{t+m+L}|^2 \tag{4}$$

where L is the length of a symbol, t is the sample index of the complex signal x, and x^* denotes the complex conjugate of x. Next, $P(d)$ and $R(d)$ are used to calculate a timing metric $M(d)$:

$$M(d) = \frac{|P(d)|^2}{R(d)^2} \tag{5}$$

The timing metric $M(d)$ essentially calculates a normalized autocorrelation of length L over two symbols, which will be maximal when two consecutive symbols are encountered in the signal. An added advantage of this approach is that any errors introduced by the channel or SDR (e.g. interference, Carrier Frequency Offset (CFO) and Sampling Frequency Offset (SFO) errors), consistently influence both symbols and therefore minimally affect the result

[4] `https://github.com/rpp0/gr-lora`

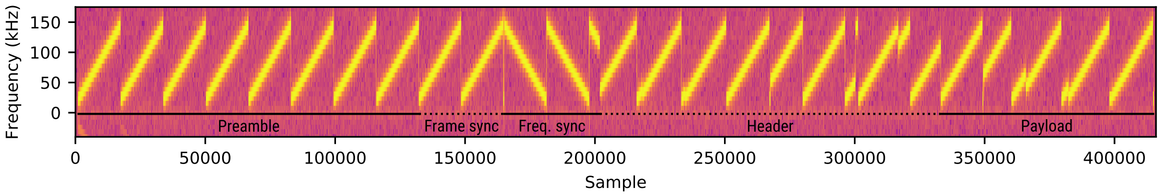

Figure 3: Annotated spectogram of an example LoRa signal transmitted with the RN2483 LoRa transceiver using SF 11 and CR 5, and received with a USRP B210 SDR.

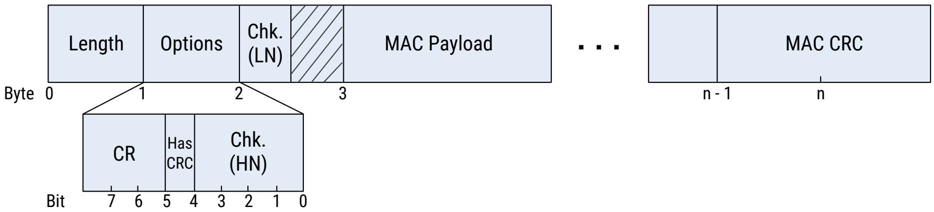

Figure 4: The fields of the LoRa PHY layer.

of the correlation. To efficiently compute Equation 3 – 5 in software, we use Single Instruction, Multiple Data (SIMD) instructions provided by Vector Optimized Library of Kernels (VOLK). Figure 6 (a) shows the resulting value of the timing metric $M(d)$ when evaluated for a complex LoRa signal. Observe that the function reaches a plateau around sample 2,500, which confirms the presence of a preamble.

Although the Schmidl-Cox algorithm can determine the presence of a preamble effectively, the plateau of the timing metric leads to uncertainty as to the start of the symbol (Schmidl and Cox, 1997). Wang et al. proposed a variation on the Schmidl-Cox algorithm where $M(d)$ is subtracted with a time-delayed version $M_2(d)$ of itself (Wang et al., 2003). Consequently, the plateau becomes a peak as shown in Figure 6 (b), making it possible to take the *argmax* of the timing metric in order to estimate the start of the preamble. However, for LoRa signals, this estimate is not sufficiently accurate, as shown in Figure 6 (c).

To solve this problem, we only use the standard Schmidl-Cox metric with a threshold to assert that the second symbol window is located anywhere inside the preamble. Next, we generate an ideal, locally synthesized base chirp and calculate its instantaneous frequency $\omega_l(t)$, as well as the instantaneous frequency of the received LoRa signal $\omega(t)$. Finally, a sliding window normalized cross-correlation is performed, and the index of the maximum value of the cross-correlation is chosen as the starting point of the symbol:

$$\text{symbol start} = \underset{i \in \{0,1,\ldots L\}}{\arg\max}\ (\omega_l \star \omega)(i) \tag{6}$$

The result of this operation is visualized in Figure 6 (d). Note that by performing the cross-correlation on the instantaneous frequency of the signals instead of their complex values, any CFO errors imparted by the channel are automatically mitigated similarly to the Schmidl-Cox algorithm. Thus, the accuracy of the synchronization is not affected by the CFO. On the contrary, if one would consider the complex-valued signals, a correction of frequency errors introduced by the channel and SDR would have to be performed before the signal can be cross-correlated with the locally synthesized chirp.

At last, in order to verify the correctness of the time synchronization, we threshold against the maximum correlation coefficient between the instantaneous frequency of the locally generated chirp and received chirp. The LoRa frame is rejected if the correlation coefficient falls below a certain tolerance value, since this indicates a failed synchronization or false positive during the detection stage (see Section 3.1).

3.2 Demodulation

Following synchronization, the receiver can demodulate the chip values as discussed in Section 2. However, the FFT-based demodulation approach specified in (Seller and Sornin, 2014) is sensitive to frequency offset errors, which cause the magnitudes of the FFT (and thus the chip values) to shift. Therefore, an accurate frequency synchronization is required. Furthermore, this synchronization must be applied for each LoRa channel separately in order to fulfill our requirement of multi-channel decoding motivated in Section 1.

Since channelization and separate processing of each channel is an expensive operation to perform in

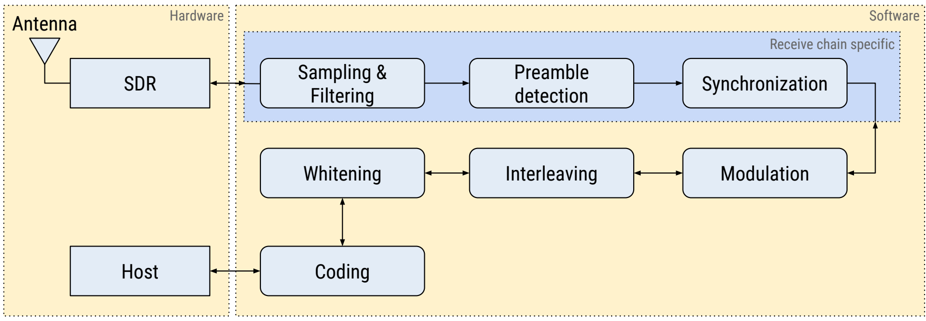

Figure 5: An overview of the LoRa decoder components, showing the various logical processing blocks required for the transmission and reception of baseband I/Q samples with an SDR.

software, we have developed a novel demodulation technique that is independent of the frequency. Our technique removes the need for frequency corrections and allows to decode LoRa frames in real time on all channels and without additional processing overhead, but at the cost of a reduced robustness compared to the FFT approach discussed in Section 2.1. This tradeoff will be discussed in Section 4.

In our methodology, we first calculate the instantaneous angular frequency $\omega[t] = \frac{d\varphi[t]}{dt}$. We then smooth and decimate $\omega[t]$ with a constant decimation factor of $\frac{s_f T}{2^{SF}}$, where s_f is the sampling frequency. This ensures that the number of samples in $\omega[t]$ is equal to 2^{SF}. Subsequently, the digital gradient of f is calculated:

$$D_t[\omega[t]] = \omega[t+1] - \omega[t] \tag{7}$$

This operation can be intuitively seen as a high pass filter on the instantaneous frequency, or as the second order derivative of the phase. Since the frequency of a base chirp linearly increases with k, i.e. $\omega(t) = kt + f_0$, its derivative $\omega'(t)$ is equal to k. For a modulated chirp however, D_t will exhibit a sharp peak at the transition from high to low frequency. If present, the position of the peak indicates the time shift $\hat{t}$. Otherwise, the time shift is equal to 0 (base chirp).

3.3 Decoding

In the decoding stage, the chip values are deinterleaved to form codewords of $4 + CR$ bits. The first 8 codewords of a frame can be directly decoded to form the PHY-layer header. On the other hand, we found that the payload symbols must be dewhitened first. Although the datasheet released by Semtech specifies the usage of a 9-bit LFSR, a different and unknown whitening LFSR appears to be implemented in practice (Knight, 2016; Blum, 2017). We have reverse engineered the whitening sequence using the following approach.

If we represent the whitening process as $c_w^{(j)} = c^{(j)} \oplus w^{(j)}$ with c_w the whitened codeword, c the unwhitened codeword, w the output of the LFSR and j the byte index, we can determine $w^{(j)}$ by transmitting a known codeword $c^{(j)}$ and calculating $w^{(j)} = c_w^{(j)} \oplus c^{(j)}$. For example, a payload with all codewords set to zero will result in $w^{(j)} = c_w^{(j)} \oplus 0$, or the whitening sequence itself. Hence, after transmitting a payload consisting of all zeros, the resulting whitening sequence can be retrieved and stored in a lookup table.

With knowledge of the whitening sequence w, the last step after dewhitening is to perform Hamming decoding on the codewords. We found that in LoRa transceivers, the data bits are positioned at bit indices 0, 1, 2, and 3 of a byte. This is in contrast to standard Hamming which uses indices 1, 2, 3, and 5 as data bits. This mapping is graphically depicted in Figure 7. After extraction of the data bits and error correction or detection based on the present parity bits, the demodulator outputs the data to a UDP socket for further processing by higher-layer applications.

3.4 Clock drift correction

The crystal oscillators in the SDR and LoRa transceiver inherently have a relative and unknown clock drift, which causes a loss of synchronization over time. This is especially problematic for long payloads in combination with higher SFs due to the symbol lengths in these configurations. To correct for the clock drift, we propose a blind estimation technique[5]

[5] Although the LoRa patent specifies the usage of "pilot" symbols for tracking timing (Seller and Sornin, 2014), these symbols appear to be absent in practice. We therefore need to make use of blind estimation techniques.

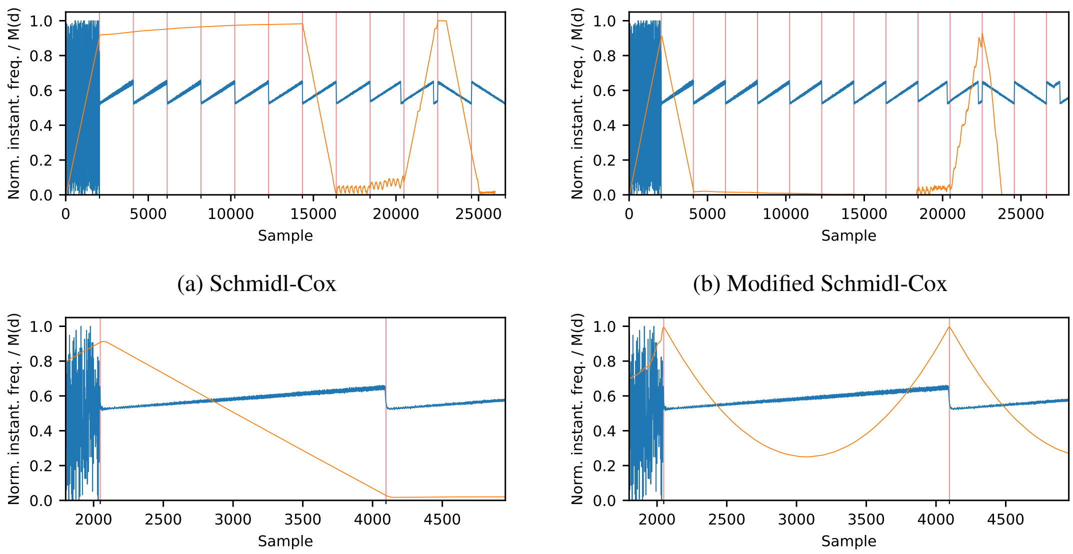

(a) Schmidl-Cox

(b) Modified Schmidl-Cox

(c) Modified Schmidl-Cox (zoomed)

(d) Our sync. algorithm (zoomed)

Figure 6: Normalized instantaneous frequency of a LoRa signal (blue) and the normalized Schmidl-Cox timing metric $M(d)$ (orange). The vertical red lines indicate the symbol window length L. In (a), the timing metric reaches a plateau upon encountering two consecutive and identical symbols. A modified version (b) results in a single peak at the first symbol, but is insufficiently accurate to determine the start of the preamble (c). Our synchronization using the normalized cross-correlation of the instantaneous frequency (d) shows a sharp peak at the start of each preamble symbol.

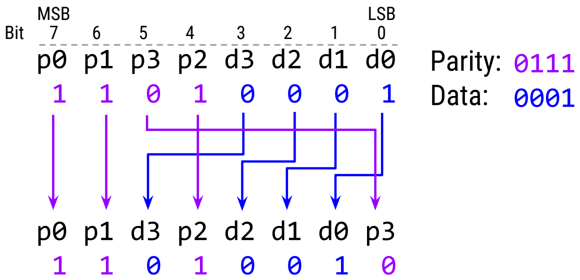

Figure 7: The bit mapping of an example Hamming codeword used in LoRa (top) to a standard Hamming code (bottom), for a CR of 4 and data `0x1`.

that exploits oversampling of the transmitted signal at a rate of N.

As a first step, our technique requires an accurate initial acquisition of the timing offset using the algorithm discussed in Section 3.1. Assuming that the timing error *per symbol* Δt, measured in number of samples, satisfies the inequality $|\Delta t| < \frac{N}{2}$, we can determine Δt as follows:

1. The symbol is demodulated normally as described in Section 3.2, in order to obtain the chip value i and the time shift $\hat{t}$.
2. At the receiver, a locally generated ideal upchirp is now modulated using i, which introduces a time shift of $\hat{t}_l$ on the local signal (see Section 2).
3. Since the locally generated chirp is not subject to relative clock drift, the timing error is: $\Delta t = \hat{t}_l - \hat{t}$. The receiver can now correct $\hat{t}$ by adding a time offset of Δt to the received signal.

Note that if the timing error for a single symbol $|\Delta t| \geq \frac{N}{2}$, the decoder will incorrectly determine the chip value i and therefore propagate the error to subsequent symbols. For this reason, we interpolate from $\hat{t}$ to $\hat{t} + \Delta t$ rather than setting the value directly. This mitigates the effect of single-symbol demodulation errors on the clock drift correction algorithm. A higher oversampling rate N allows for more fine-grained timing error corrections at the cost of increased processing overhead.

4 EVALUATION

Our demodulator was evaluated in a lab setup using different SDR models and LoRa hardware. More specifically, we have performed tests with the RN2483, SX1272 and RFM96 configured as transmitters and the Ettus B210 USRP, HackRF, and RTL-SDR configured as receivers. Each test was performed using a carrier frequency of 868.1 MHz, a sample rate of 1 Msps, and a distance between the transmitter and receiver of about 1 meter. The source code required for reproducing the test results and datasets from the accuracy experiments are publicly available on Github[6].

4.1 Compatibility

In a first experiment, we evaluated the compatibility of our decoder with hardware LoRa transceivers. Here, we used the USRP as the receiver and RN2483, SX1272 and RFM96 as transmitters. The compatibility was evaluated by transmitting the payload "`0123456789abcdef`" 100 times for all possible combinations of CR and SF, and checking the number of correctly decoded frames. A configuration is considered compatible when transmitted LoRa frames are consistently correctly decoded under ideal channel conditions and a high Signal-to-Noise Ratio (SNR).

The results of this experiment are shown in Table 1. Observe that the only incompatible configurations are SF 11 and SF 12 for the RFM96 transceiver. After a manual inspection, we found that the cause of this incompatibility is due to the fact that the RFM96 transceiver does not enable the reduced data rate mode as mandated in the LoRa specification (Semtech, 2015b, p. 28). In fact, even when transmitting a message from the RFM96 to either the hardware SX1272 or RN2483 hardware transceivers, the resulting frame is always corrupted for SF 11 and SF 12. When we manually disabled reduced data rate mode in our decoder, we achieved full compatibility with all devices. This confirms that the issue lies within the hardware implementation of the RFM96, and shows that our decoder can be used to troubleshoot incompatibilities between LoRa devices from different vendors.

4.2 Accuracy

In the accuracy experiments, we measured the Packet Error Rate (PER), i.e. the ratio of erroneous packets received over the total number of packets transmitted, for a fully compatible transmitter configured with SF 7 and CR 4. We also artificially introduce two types of channel distortions to the I/Q signal at the receiver, namely Gaussian white noise and CFOs.

Figure 8 shows the effect of artificial Gaussian white noise on the decoding accuracy when using a SF of 8 and CR of 4, the RN2483 as a transmitter, and the HackRF, RTL-SDR and USRP SDRs as receivers. The receivers were each configured with a receive gain of 10 dB, and the transmit power of the RN2483 was configured to 1 dB. Note that even so, the effective receive gain between the SDRs differs due to their different hardware and antenna designs.

[6] `https://github.com/rpp0/lora-decoder-paper`

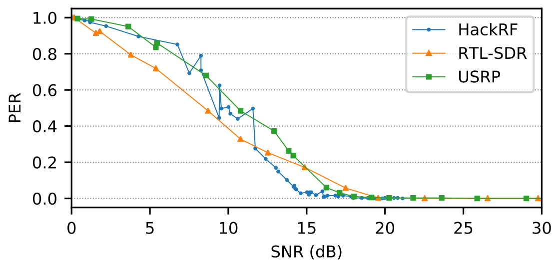

Figure 8: The effect of artificial Gaussian white noise on the accuracy of the decoder. The PER of our decoder for all evaluated SDRs approaches 0 around a SNR of 20 dB.

From the figure we can derive that a SNR around 20 dB is at least required in order to obtain a PER of 0 for all SDRs.

In Figure 9 (a), we used the USRP to add Gaussian noise at the *transmitter* instead of the receiver in order to compare our decoder (RTL-SDR) with a hardware LoRa transceiver (RN2483). For this experiment, both receivers were placed at an equal distance from the USRP, and 100 frames with a payload of "`0123456789abcdef`" were transmitted to calculate the PER. Observe that the RN2483 is still capable of receiving frames well below the noise floor, whereas our decoder stops receiving any frames at 0 dB SNR. At this point, the transient of the gradient cannot be detected by our gradient-based decoding algorithm due to the presence of excess noise.

On the other hand, when we introduce a CFO instead of Gaussian noise to the transmitted signal, our decoder outperforms the hardware for a CFO larger than 50 kHz or when transmitting at a different channel as shown in Figure 9 (b)[7]. The hardware device must be retuned in order to capture frames from a different channel, whereas our decoder is capable of capturing frames from multiple channels simultaneously.

Based on these observations, we conclude that our decoding technique essentially trades flexibility (i.e., being able to decode multiple channels simultaneously at no additional cost) for an increased sensitivity to Gaussian noise. Although the increased sensitivity to noise reduces the functioning range of the receiver, the flexibility of our approach allows for building a fully compatible and multi-channel LoRa monitoring device at a very low cost. We therefore believe our software decoder is especially suited for research purposes. In fact, in a previous work, the authors have used the discussed techniques to extract PHY-layer

[7] Note that at 125 kHz, the PER of the RN2483 decreases momentarily back to 0.2. This could possibly be explained by the CFO causing the FFT peak to wrap back to an approximately correct position.

Table 1: Results of the compatibility experiment, showing the LoRa transceivers and configurations for which our decoder was able to successfully decode frames.

Transceiver	SF 7, CR 1	SF 7, CR 2	SF 7, CR 3	SF 7, CR 4	SF 8, CR 1	SF 8, CR 2	SF 8, CR 3	SF 8, CR 4	SF 9, CR 1	SF 9, CR 2	SF 9, CR 3	SF 9, CR 4	SF 10, CR 1	SF 10, CR 2	SF 10, CR 3	SF 10, CR 4	SF 11, CR 1	SF 11, CR 2	SF 11, CR 3	SF 11, CR 4	SF 12, CR 1	SF 12, CR 2	SF 12, CR 3	SF 12, CR 4	Implicit
Custom module (RN2483)	✓	✓	✓	✓	✓	✓	✓	✓	✓	✓	✓	✓	✓	✓	✓	✓	✓	✓	✓	✓	✓	✓	✓	✓	N/A
Pycom LoPy (SX1272)	✓	✓	✓	✓	✓	✓	✓	✓	✓	✓	✓	✓	✓	✓	✓	✓	✓	✓	✓	✓	✓	✓	✓	✓	N/A
Dragino Pi HAT (RFM96)	✓	✓	✓	✓	✓	✓	✓	✓	✓	✓	✓	✓	✓	✓	✓	✓	✗	✗	✗	✗	✗	✗	✗	✗	✓*

*Only device in our possession with an API for sending frames in implicit mode. A custom header appears to be transmitted by the RFM96 in this mode.

features from LoRa signals and fingerprint individual transceivers (Robyns et al., 2017).

5 RELATED WORK

A high-level system architecture overview of LoRa is given by Centenaro et al. (Centenaro et al., 2016). Sikken has provided a general overview of the LoRa frame structure and decoding stages, but does not discuss the low level details of the modulation (Sikken, 2017). Goursaud et al. have provided a detailed and formal analysis of LoRa modulation, but do not discuss the interleaving, whitening and coding (Goursaud and Gorce, 2015).

A first complete analysis of the LoRa PHY was presented by Knight (Knight, 2016). However, in their work, it is assumed that the dewhitening operation is performed before deinterleaving, that the header is whitened, and that a different interleaving pattern is used than the diagonal interleaving specified in (Seller and Sornin, 2014). Based on our own experiments, we concluded that these claims are inaccurate. A decoder named `gr-lora` was developed based on their analysis, but appears to only be able to decode short frames transmitted without a header. We believe this limitation is the result of errors made during their reverse engineering process.

Other software LoRa decoders for SDRs have been developed by Blum et al. (Blum, 2017) and by Project Sdrangelove (RTL-SDRangelove, 2017). However, we were unable to decode any frames transmitted by hardware LoRa transceivers using these decoders. Finally, at the time of writing, none of the decoders in other works have developed a clock drift correction algorithm for decoding long LoRa frames.

Besides work on LoRa, GNU Radio based decoders have previously been developed to decode protocols such as Global System for Mobile Communications (GSM) (Alyafawi et al., 2014; Krysik, 2017), Long Term Evolution (LTE) (Demel et al., 2015), and 802.11 (Bloessl et al., 2013b; Vo-Huu et al., 2016) using SDRs.

6 CONCLUSIONS AND FUTURE WORK

In this paper, we have provided an in-depth examination of the LoRa PHY layer, and demonstrated our open source LoRa software decoder, which is implemented using the GNU Radio framework. Our decoder can be used in real time with inexpensive SDRs such as the RTL-SDR, and is able to interoperate with existing LoRa transceivers. A set of frequency invariant techniques for the detection, demodulation, and clock drift correction of LoRa frames were introduced, which result in the capability to decode multiple channels simultaneously in real time, at the cost of an increased sensitivity to noise compared to COTS LoRa radios. Our evaluation shows that a SNR of at least 20 dB is required for the PER to approach 0.

In future work, a number of aspects of the decoder can be further improved upon. Most importantly, the robustness of the decoder could be improved to approach the performance of LoRa hardware, which is a challenging problem given the limited available resources and timing constraints in real-time software decoders. Another scenario that was not yet considered in this work is the handling of collisions between LoRa frames, which could occur on a busy channel. Finally, we hope that the access to the PHY layer provided by our work will support the development of future improvements in context of LoRa.

ACKNOWLEDGEMENTS

This research was funded by a Ph.D. Grant of the Research Foundation Flanders (FWO), grant number 1S14916N.

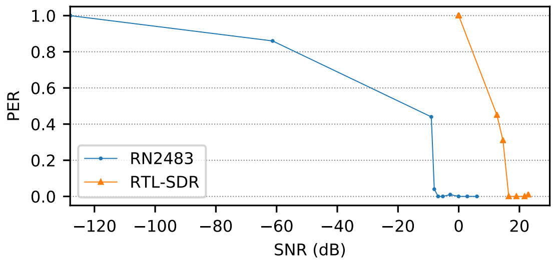

(a)

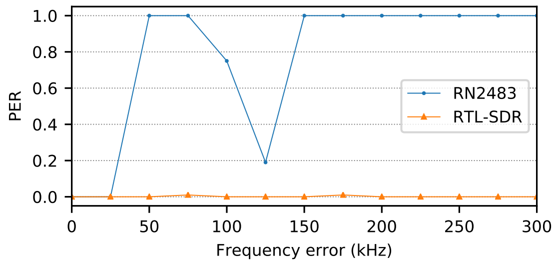

(b)

Figure 9: Comparison between the RTL-SDR using our software decoder versus a hardware RN2486 LoRa transceiver in terms of resistance to Gaussian noise (a) and resistance to frequency offset errors (b). Due to the properties of our gradient-based decoding algorithm, our decoder is shown to be unaffected by frequency errors at the cost of a significantly higher sensitivity to Gaussian noise compared to the RN2483.

REFERENCES

3GPP (2017). LTE Release 13. `http://www.3gpp.org/release-13`. Accessed: 9 October 2017.

Alyafawi, I., Dimitrova, D. C., and Braun, T. (2014). Real-time passive capturing of the GSM radio. In *IEEE International Conference on Communications (ICC)*, pages 4401–4406. IEEE.

Ben Hamida, E., Chelius, G., and Gorce, J. M. (2009). Impact of the physical layer modeling on the accuracy and scalability of wireless network simulation. *Simulation*, 85(9):574–588.

Bloessl, B., Leitner, C., Dressler, F., and Sommer, C. (2013a). A GNU radio-based IEEE 802.15. 4 testbed. *12. GI/ITG KuVS Fachgespräch Drahtlose Sensornetze (FGSN 2013)*, pages 37–40.

Bloessl, B., Segata, M., Sommer, C., and Dressler, F. (2013b). An IEEE 802.11 a/g/p OFDM Receiver for GNU Radio. In *Proceedings of the second workshop on Software radio implementation forum*, pages 9–16. ACM.

Blum, J. (2017). LoRa SDR project. `https://github.com/myriadrf/LoRa-SDR`. Accessed: 10 October 2017.

Centenaro, M., Vangelista, L., Zanella, A., and Zorzi, M. (2016). Long-Range Communications in Unlicensed Bands: the Rising Stars in the IoT and Smart City Scenarios. *IEEE Wireless Communications*, 23.

Danev, B., Zanetti, D., and Capkun, S. (2012). On physical-layer identification of wireless devices. *ACM Computing Surveys (CSUR)*, 45(1):6.

Demel, J., Koslowski, S., and Jondral, F. K. (2015). A LTE receiver framework using GNU Radio. *Journal of Signal Processing Systems*, 78(3):313–320.

Goursaud, C. and Gorce, J.-M. (2015). Dedicated networks for IoT: PHY/MAC state of the art and challenges. *EAI endorsed transactions on Internet of Things*.

Gray, F. (1953). Pulse code communication. US Patent 2,632,058.

i-SCOOP (2017). Wireless Internet of Things connectivity: LPWAN IoT forecasts 2017. `https://www.i-scoop.eu/internet-of-things-guide/iot-spending-2020/wireless-iot-lpwan-forecasts-predictions-2017/`. Accessed: 10 October 2017.

Knight, M. (2016). Reversing LoRa: Exploring Next-Generation Wireless. GRCon.

Krysik, P. (2017). GNU Radio blocks and tools for receiving GSM transmissions. `https://github.com/ptrkrysik/gr-gsm`. Accessed: 10 October 2017.

LoRa Alliance (2017). LoRa Alliance home page. `https://www.lora-alliance.org/`. Accessed: 9 October 2017.

Mann, S. and Haykin, S. (1991). The chirplet transform: A generalization of Gabor's logon transform. *Vision Interface '91*, pages 205–212. ISSN 0843-803X.

Mezzavilla, M., Dutta, S., Zhang, M., Akdeniz, M. R., and Rangan, S. (2015). 5G mmwave module for the ns-3 network simulator. In *Proceedings of the 18th ACM International Conference on Modeling, Analysis and Simulation of Wireless and Mobile Systems*, pages 283–290. ACM.

Microchip Technology Inc. (2015). Low-Power Long Range LoRa Technology Transceiver Module. `http://ww1.microchip.com/downloads/en/DeviceDoc/50002346A.pdf`. Accessed: 10 October 2017.

Robyns, P., Marin, E., Lamotte, W., Quax, P., Singelée, D., and Preneel, B. (2017). Physical-layer fingerprinting of LoRa devices using supervised and zero-shot learning. In *Proceedings of the 10th ACM Conference on Security and Privacy in Wireless and Mobile Networks*, pages 58–63. ACM.

RTL-SDRangelove (2017). Github project page. `https://github.com/hexameron/rtl-sdrangelove`. Accessed: 10 October 2017.

Schmidl, T. M. and Cox, D. C. (1997). Robust frequency and timing synchronization for OFDM. *IEEE transactions on communications*, 45(12):1613–1621.

Seller, O. and Sornin, N. (2014). Low power long range transmitter. EP Patent App. EP20,130,154,071.

Semtech (2012). Semtech Acquires Wireless Long Range IP Provider Cycleo. `http://investors.semtech.`

com/releasedetail.cfm?ReleaseID=655335. Accessed: 9 October 2017.

Semtech (2015a). LoRa Modulation Basics. http://www.semtech.com/images/datasheet/an1200.22.pdf. Accessed: 9 October 2017.

Semtech (2015b). SX1272/73 - 860 MHz to 1020 MHz Low Power Long Range Transceiver Datasheet. http://www.semtech.com/images/datasheet/sx1272.pdf. Accessed: 10 October 2017.

Sigfox (2017). Sigfox home page. https://www.sigfox.com/. Accessed: 9 October 2017.

Sikken, B. (2017). Decoding LoRa. https://revspace.nl/DecodingLora. Accessed: 10 October 2017.

Sklivanitis, G., Gannon, A., Batalama, S. N., and Pados, D. A. (2016). Addressing next-generation wireless challenges with commercial software-defined radio platforms. *IEEE Communications Magazine*, 54(1):59–67.

Sornin, N., Luis, M., Eirich, T., Kramp, T., and Hersent, O. (2015). LoRaWAN™ Specifications. *LoRa™ Alliance*.

The Things Network (2017). Gateway coverage map. https://www.thethingsnetwork.org/map. Accessed: 10 October 2017.

Vo-Huu, T. D., Vo-Huu, T. D., and Noubir, G. (2016). Fingerprinting Wi-Fi Devices Using Software Defined Radios. In *Proceedings of the 9th ACM Conference on Security & Privacy in Wireless and Mobile Networks*, pages 3–14, New York, NY, USA. ACM.

Wang, K., Faulkner, M., Singh, J., and Tolochko, I. (2003). Timing synchronization for 802.11 a WLANs under multipath channels. In *Proc. ATNAC*, volume 2004.

Weightless (2017). Weightless home page. http://www.weightless.org/. Accessed: 9 October 2017.

Wi-Fi Alliance (2017). Wi-Fi HaLow home page. https://www.wi-fi.org/discover-wi-fi/wi-fi-halow. Accessed: 9 October 2017.